On the Structure Elucidation Using Ion Mobility Spectrometry and Molecular Dynamics

F. A. Fernandez-Lima, H. Wei, Y. Q. Gao, and D. H. Russell*

Department of Chemistry, Texas A&M University, College Station, Texas, 77843

A new approach is described for the elucidation of gas-phase peptide ion structures combining ion mobility spectrometry (IMS) data and molecular dynamics (MD)−cluster analysis (CA) prediction. The new approach is based on the determination of the gas-phase ion structure identity vectors (e.g., structure and population vectors) that generate the total conformational space of the gas-phase ion as a function of the IMS experimental conditions (e.g., field strength, pressure, bath gas temperature, and IM cell geometry). Two methods to efficiently sample the gas-phase conformational space of molecular ions as a function of the effective ion temperature characteristic of the IMS experiments are described: (i) a simulated annealing MD−CA−constant temperature MD−CA, and (ii) a generalized non-Boltzmann sampling MD−free energy analysis−CA. The new theoretical method has been successfully applied to two model peptide ions (Bradykinin fragments 1-5 and 1-8, RPPGF and RPPGFSPF, respectively) for which multiple conformations sensitive to the effective ion temperature have been suggested in previous studies.

Introduction

The folding of proteins and peptides in a physiological environment depends on numerous factors (e.g., electrostatic interactions, intermolecular interactions with the solvent, entropic effects, intramolecular hydrogen bonding, and van der Waals interactions). In nature, protein folding occurs in a variety of environments, ranging from pure aqueous to hydrophobic and low dielectric conditions.[1−3] Thus, solvent-free studies may be interesting from a fundamental point of view, as they provide means of separating solvation effects from intrinsic properties of peptide chains and proteins. For example, solvent-free studies may provide new approaches to studies of "non-native" structure that can be used to evaluate protein folding/unfolding models[4] as well as nucleation and growth.[5]

With the advent of soft ionization techniques (e.g., ESI and MALDI), the study of intrinsic conformational and thermochemical properties of anhydrous peptides and proteins in the gas phase are growing rapidly.[6−9] While most structural applications have been directed to protein identification by the determination of the primary structure (sequence information),[10] significant progress has been made in developing techniques directed toward conformational analysis. For example, hydrogen/deuterium (H/D) exchange studies have been used to probe the number of exchangeable hydrogen atoms as a measure of the folding degree of a targeted protein.[11−16] Several laboratories have developed IR spectroscopic techniques to study secondary structural elements of small peptides, based on comparisons of theoretically estimated vibrational frequencies of candidate structures.[17,18] Ion mobility spectrometry (IMS) combined with MD simulations has proven to be the most versatile technique for conformational analysis of intermediate and equilibrium structures of biomolecules by measuring the ion-neutral, collision cross-section (CCS) of molecular ions.[19−21] Ion mobility measurements have been used to explore molecular dynamics and follow structural changes occurring on the millisecond time scale by comparison to calculated CCS of candidate structures under controlled condition (e.g., reactive/inert, polar/nonpolar

bath gas at different temperatures).[22−24] A major difficulty in simulating processes occurring in IMS experiments is the long time scale over which structural rearrangements may occur (approximately a few milliseconds) whereas molecular dynamics simulations are typically limited to nanoseconds.[25−27] Although a number of enhanced sampling methods have been developed to reduce the computation time,[28−36] further improvements are needed to efficiently correlate the theoretical results with available experimental data. A good theoretical description of the IMS experiments will ultimately lead to the understanding of the building blocks that govern the structural preference of peptides and proteins under controlled experimental conditions.

In the present paper, we describe a molecular dynamics (MD)−cluster analysis (CA) approach for the determination of the gas-phase ion identity vectors (e.g., structure and population vectors) that generate the total conformational space of the gas-phase ion as a function of the IMS experimental conditions (e.g., field strength, pressure, bath gas temperature, and IM cell geometry). Two methods are described to generate the gas-phase ion identity vectors: (i) a simulated annealing MD−CA−constant temperature MD−CA, and (ii) a generalized non-Boltzmann sampling MD−free energy analysis−CA. The new theoretical method is been successfully applied to two model peptide ions (Bradykinin fragment BK 1-5 and BK 1-8, RPPGF and RPPGFSPF, respectively) for which multiple conformations sensitive to the effective ion temperature have been suggested in previous studies.[37]

Experimental Method

The experimental details of the MALDI−IM-MS instrumentation and data acquisition used in this study have been described elsewhere.[38−41] Briefly, ions were formed in an IM drift cell by irradiating the sample plate with the output from a microcrystal Nd:YAG laser (355 nm, Powerchip Nanolaser, JDS Uniphase Corp.), operating at a pulse rate of 300 Hz. The desorbed ions were separated according to their drift time in an IM cell maintained at a pressure of ∼3.0 Torr of helium and field strength/pressure ratio (E/p) of 10−40 V cm^{-1} Torr^{-1}. To verify the components of the IM peaks (e.g., *m/z* and peptide

---

sequence), ions exiting the IM cell were activated by collision induced dissociation (CID) in the IM-MS interface, and then focused into the ion source of an orthogonal time-of-flight mass spectrometer equipped with an electrostatic mirror (mass resolution of 1500−3000). In all experiments, the temperature of the bath gas was ca. 300 K. The ion−neutral collision cross sections (CCS) were reported according to the method described by Mason and McDaniel.[42] A fullerene mixture was used as a CCS reference.[43,44] The experiments were performed using a laser power near the ion desorption threshold to minimize peak broadening of the arrival time distribution (ATD) due to space charge effects.[45]

The peptides BK 1-5 (RPPGF) and BK 1-8 (RPPGFSPF) used in these studies were purchased from Gen Script Corp. (Piscataway, NJ) and used without further purification. The α-cyano-4 hydroxycinnaminic acid was purchased from Sigma Aldrich (St. Louis, MO). HPLC grade methanol and deionized (Milli-Q Water System, Millipore, Billerica) water were used for all experiments. The MALDI samples were prepared using the dried droplet method with α-cyano-4-hydroxycinnaminic acid as the matrix with a matrix-to-analyte molar ratio of 400: 1.

Theoretical and Computational Details

Description of the Ion Dynamics in the IMS Experiments. The motions and chemical reactions of a swarm of charged particles in neutral gases have been described elsewhere.[42,46−49] The main limitations of the theoretical description have been that primarily a general theory must encompass all reasonable ion−molecule interaction potentials and mass ratios and that it must also handle both low-field conditions, i.e., ions with a near-Maxwell−Boltzmann velocity distribution, and high-field conditions, i.e., ions with a non-Maxwell−Boltzmann velocity distribution.[42]

The transport coefficients of molecular ion−neutral systems and cross sections governing the ion−neutral collisions may be obtained by solving the Wang Chang−Uhlenbeck−de Boer (WUB) equation.[50] This equation is a generalization of the Boltzmann kinetic equation that takes into account the presence of anisotropic intermolecular forces and internal degrees of freedom that can result in inelastic collisions. Nevertheless, it should be noted that it does not take into account the quantum-mechanical interference effects that can occur when internal states are degenerate,[51] but such effects are relatively small and mainly contribute at low temperatures. The essential feature of the kinetic theory for molecular systems is that the ions present in a drift tube are allowed to have a different temperature than the neutrals, as a result of the electric field (E) acting on them, analogous to the atomic two temperature kinetic theory.[52] This theory indicates that the mobility K of an atomic ion drifting in an atomic neutral gas is given by[53]

$$K = \frac{v_d}{E} = \frac{3q}{8N}\left(\frac{\pi}{2\mu k_b T_{eff}}\right)^{1/2}\frac{1+\alpha}{\Omega^{(1,1)}(T_{eff})} \quad (1)$$

$$\frac{3}{2}k_b T_{eff} = \frac{3}{2}k_b T_{BG} + \frac{1}{2}Mv_d^2(1+\beta) \quad (2)$$

Here v_d is the ion drift velocity, N is the gas number density, M is the neutral mass, q is the ion charge, μ is the ion−neutral reduced mass, k_b is the Boltzmann's constant, and $\Omega^{(1,1)}(T_{eff})$ is the temperature dependent momentum transfer collision inte-

gral.[53] The small correction terms α and β may be calculated precisely if the ion−neutral interaction potential is known.[54] The effective ion temperature (T_{eff}) is the temperature that characterizes the average ion-neutral collision energy in the center-of-mass frame.

When the ions or neutrals are molecular rather than atomic, eqs 1 and 2 must be modified to account for anisotropic interaction potentials and inelastic collisions. A new effective ion temperature T'_{eff} must be used in place of T_{eff}, to account for inelastic energy losses:[46,50]

$$K = \frac{v_d}{E} = \frac{3q}{8N}\left(\frac{\pi}{2\mu k_b T'_{eff}}\right)^{1/2}\frac{1+\alpha'}{\Omega^{(1,1)}(T'_{eff})} \quad (3)$$

$$\frac{3}{2}k_b T'_{eff} = \left[1 + \frac{M}{m}\xi\right]^{-1}\left[\frac{3}{2}k_b T_{BG} + \frac{1}{2}Mv_d^2(1+\beta')\right] \quad (4)$$

where α' and β' are correction terms that are probably of the same order of magnitude as α and β, respectively, and ξ is a dimensionless ratio of collision integrals that characterizes the fractional energy loss due to inelastic collisions.[54] When E/p is small $\xi \rightarrow 0$, and eq 4 reduces to eq 2, i.e., even molecular ion−neutral systems should obey the prediction that K is a function only of T_{eff} for values of T_{eff} slightly larger than T_{BG}.

A special case of great practical importance is the study of molecular ions in a pure atomic gas, where at steady state the internal temperature of the ions must be equal to the effective temperature given by eq 4. The physical description for this case is that energy is fed into the internal degrees of freedom of the ions by collisions with the atomic neutrals; the source of the ion internal energy is translational motion. Energy leaks from both the internal and translational degrees of freedom of the ions only through the translational motion of the neutrals. Since the leak is the same for both forms of energy, and since the internal energy is fed by translation, it is not surprising that the internal and effective translational temperatures are equal in steady state.[46]

To gain a better understanding of the ion dynamics inside an IM cell, ion dynamic simulations of elastic molecular ion−atomic neutral collisions were performed to illustrate the elastic effective ion temperature ($T_{eff}^{elastic} = T'eff(\xi \rightarrow 0)$) dependence on the experimental conditions accessible in the IMS experiment (e.g., field strength, pressure, bath gas temperature, and IM cell geometry). In the IM cell, a gas pressure of ∼3.0 Torr of helium and a E/p of 10−40 V cm^{-1} Torr^{-1} were considered. The pressure gradient was modeled using the Fluent 6.2.16 (Fluent, Inc., Lebanon, NH) computer software.[55] The pressure profile was incorporated into a Simion 3D[56] user developed program, which was used to determine the ion trajectories along the IM interface axis. For these simulations we assumed ideal gas behavior where the specific heat capacity (c_p), thermal conductivity, and viscosity parameters are determined by a helium−helium pair interaction potential (kinetic theory). A helium−helium Lennard-Jones potential with 2.96 Å equilibrium internuclear distance and 10.98 K interaction energy (ε/k) was employed.[57] The ion trajectories in the IM cell were calculated considering an elastic hard sphere scattering model (EHSS) for the ion−helium collisions.[58]

Molecular Dynamics (MD)−Cluster Analysis (CA) Prediction. The MD−CA prediction is based on the determination of the gas-phase ion structure identity vectors (e.g., structure and population components) that generate the total conforma-
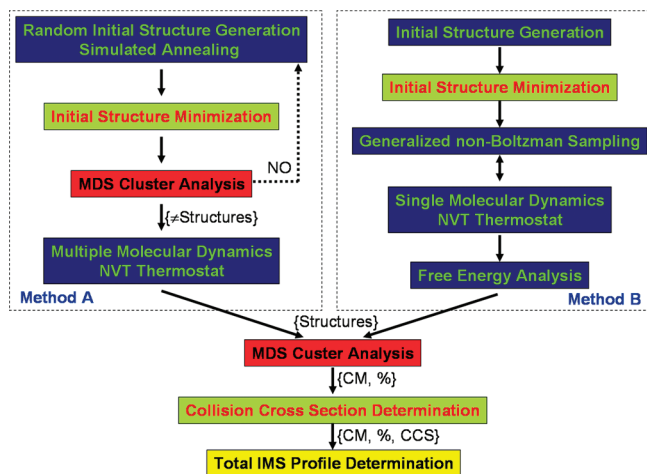
Structure Elucidation Using IMS and Molecular Dynamics

J. Phys. Chem. A, Vol. 113, No. 29, 2009 **8223**

Figure 1. Schematics of the theoretical method used to generate the representative structures of the conformational space as a function of the effective ion temperature.

tional space as a function of the IMS experimental conditions (e.g., field strength, pressure, bath gas temperature, and IM cell geometry). Two methods are used to generate the gas-phase ion structure identity vectors: (i) a simulated annealing MD−CA−constant temperature MD−CA and (ii) a generalized non-Boltzmann sampling MD−free energy analysis−CA. The MD−CA scheme is illustrated in Figure 1. The initial set of candidate structures, {structures}, generated using Method A and/or B is classified by a center of mass structure (or representative structure) and the relative abundance vector, {CM, %}, is obtained using MDS cluster analysis techniques (as described below). The CCSs of all the center of mass structures are calculated, and, considering the relative abundances of the center of mass structures, the theoretical IMS profiles are generated. This procedure is performed for different experimental conditions (e.g., E/p, T_{BG}, and IM cell geometry); i.e., the IMS profiles are generated as a function of the effective ion temperature. The particularities of each stage are further described.

Method A: Simulated Annealing and Constant Temperature MD. Method A is based on the generation of a pool of initial structures using a simulated annealing process, followed by the minimization of each structure. All the minimized structures are compared using the CA method and the {≠structures} identity vector is generated, where different input structures are stored. The components of the {≠structures} vector are then submitted to multiple molecular dynamics, using a *NVT* thermostat (fixed number of particles N, volume V, and temperature T) with a T-damping temperature routine,[59,60] at different temperature ranges to simulate the experimental conditions (e.g., effective ion temperatures of 300−500 K, with steps of 50 K).

All calculations were performed using the open force field (OFF) program and the consistent force field (version 2002) in Cerius[1] (Accelrys Inc.).[61] The force field van der Waals and Coulombic cut-in and cutoff values were set to 50 and 55 Å, respectively, using a spline function. The annealing process consisted of multiple cycles (∼50 cycles for small peptides) of 300 K−1000 K−300 K temperature ramping, in steps of 200 K with a relaxation time of 1 ps. The minimization criterion for the structure optimization was set to be high. In the multiple molecular dynamics, the temperature range for each simulation was 50 K (e.g., 300−350 K, 350−400 K, etc.), and structures were stored at intervals of 0.5 ps in the {structures} vector for

further CA processing. To guarantee the oversampling of the total conformational space, the {structures} vector typically contained 2000−2500 components for each temperature range for small peptides.

Method B: Non-Boltzmann Sampling MD. Method B is based on the extraction of structures that correspond to free energy minima out of the total conformational space. The total conformational space is generated using molecular dynamic simulations with enhanced sampling over a wide energy range by making use of a generalized (non-Boltzmann) distribution functions at multiple temperatures.[26] This approach uses a biased potential for the MD simulations generated from the generalized distribution function that, when reweighted correctly, can lead to the desired thermodynamic information. This method was shown to be efficient in free energy simulations[25] as well as in protein folding studies.[62] The {structures} vector contains ∼3000 structures randomly chosen from all the sampled structures (with correction made for each structure to reflect its probability of appearance). That is, the components of the {structures} vector are representative of the low energy states and were generated at different temperature ranges to simulate the experimental conditions (e.g., effective ion temperatures of 300−550 K, with steps of 50 K).

The Amber 99 force field[63] was utilized for all amino acid residues in the peptides included in our simulations and all the quantum mechanics (QM) calculations were carried out using Gaussian 03 program suite.[64] The partial charges on all atoms in the neutral N- and C-terminal forms of arginine and phenylalanine were derived by using the RESP method based on two conformations (extended and α-helix-like) optimized at the QM level of HF/6-31G+(d).[65,66] The corresponding electrostatic potential was also computed at the same QM level and then the charge fitting was derived with the RED program.[67]

The extended conformations of the BK 1-5 and BK 1-8 peptides were used as the initial structures. A 500 step minimization was conducted before the system was heated up to 300 K in a 20 ps MD simulation. Then, a 1 ns MD simulation was carried out to estimate the potential energy range for the entire conformational space using the AMBER 9 package.[68] Based on this approximation, a multi-Gaussian type biasing potential was introduced into the system to effectively sample all conformations, including minima and transition states.[26] At last, all conformations were collected in the following 20 ns trajectory for analyses as the biasing potential was fixed (see example in Figure 4a). The free energy vs the RMSD of the peptide backbone distribution was computed on the basis of the probability distribution of all conformations (see example in Figure 4b).

Cluster Analysis. The cluster analysis is based on the comparison of all structures and subsequent classification in clusters; i.e., structures are classified such that a given cluster contains a set of structures that are more similar to one another than to members of other clusters. Comparison between the similarities of two structures is made using the average root-mean-square deviation (RMSD) using the SUPPOSE program.[69] Average RMSD values are computed from the pairwise RMSD measured between corresponding atoms of two structures, once the corresponding atoms have been identified and the molecules have been rotated and translated as rigid bodies to the best match.

A multidimensional scaling (MDS) method is used to generate an *n*-dimensional projection of all the structures, where the interpoint distances are "close" to their average RMSD values.[70] The dimension, *n*, of the MDS space is chosen such that the
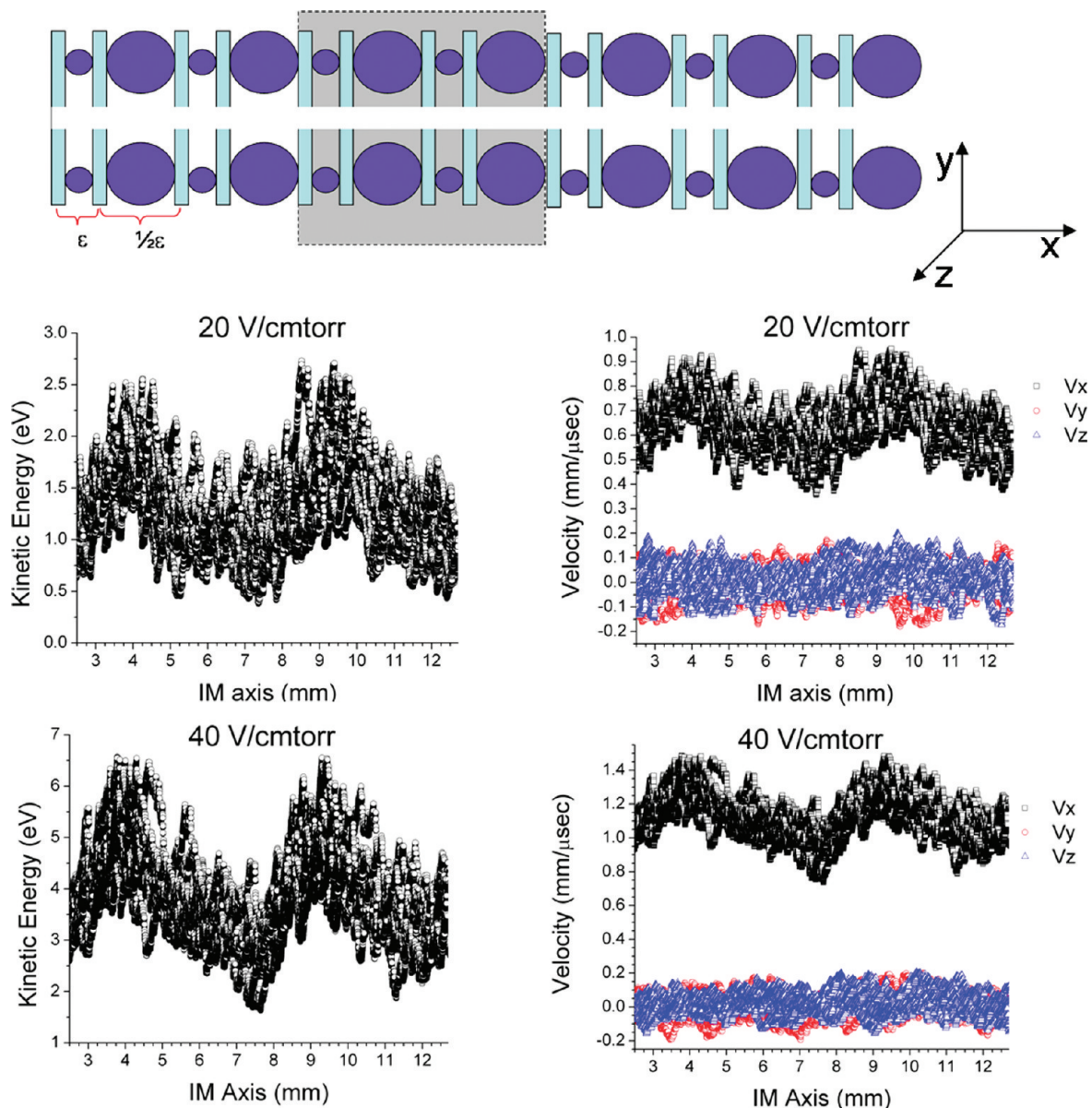
Figure 2. Plot showing kinetic energies and velocities for an ion of *m/z* 574 and CCS 170 Å^2 (equivalent to that of BK 1-5 [M + H]$^+$ ion) as a function of the position along the IM drift cell. Values correspond to the boxed, high-lighted region of the high-low field IM cell shown at the top.

TABLE 1: Effective Ion Temperature Obtained from Ion Dynamic Simulation Considering an EHSS Model for a Model Peptide Ion (Equivalent to That of BK 1-5 [M + H]$^+$ Ion) of 574 Da and 170 Å^2 Ion–Neutral Collision Cross Section Drifting in a Helium Bath Gas at T_{BG} = 300 K

E/N (10^{-21} V/m^2)	E/p (V cm^{-1} Torr^{-1})	v_d (10^2 m/s)	$T_{eff}^{elastic}$ (β'=0) (K)	$T_{eff}^{elastic}$ (β'=0.1) (K)
31	10	3.40 ± 0.56	318 ± 50	320 ± 50
62	20	6.38 ± 0.66	365 ± 46	372 ± 46
93	30	8.90 ± 0.81	427 ± 42	440 ± 42
124	40	11.14 ± 0.85	500 ± 40	520 ± 40

interpoint distances and the RMSD values correspond within a stress value below 5%.[70] The structures are classified in the *n*-dimensional MDS space using a hierarchical clustering algorithm (HCA).[71] The HCA classifies the structures without a predetermined number of clusters, which permits users to determine the natural grouping with interactive visual feedback (e.g., dendrograms, 3-D projections and/or color mosaic). The optimum number of clusters can be defined by the user or can

be determined using an iterative algorithm from a user-defined RMSD tolerance criteria within a cluster. Each cluster is represented by an identity vector in the {CM, %} identity matrix, where each vector contains the total number of members (%, cluster population) and the center of mass structure (CM, the structure most-equally distant in RMSD to all the members of the cluster). An author-developed code was implemented for the CA.

The CCSs of the CM structures were calculated using the trajectory method (TM) in the MOBCAL software.[43,44] The theoretical CCS profiles were calculated using the {CM, %, CCS} vectors and a Gaussian-like distribution, with the width of the Gaussian function defined by the experimental IM resolution.

Results and Discussion

Ion mobility spectrometry involves separation of gas-phase ions under the influence of an external electric field (*E*) and at a constant pressure (*p*) of the bath gas (BG). Under these
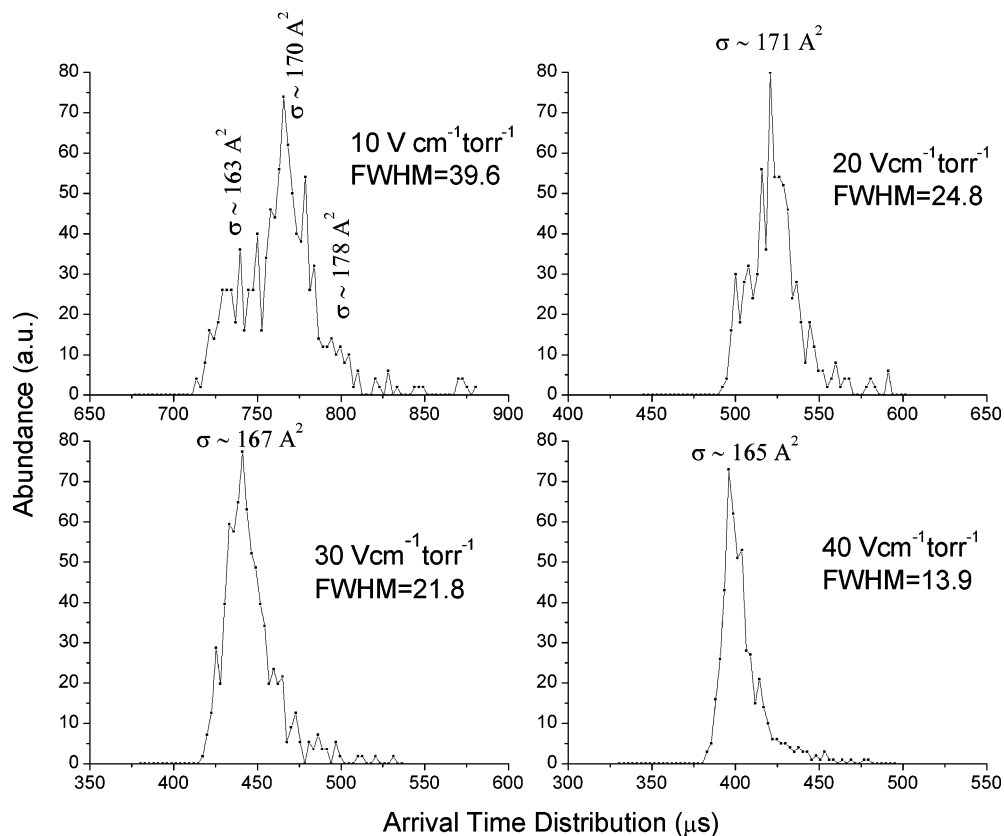
Structure Elucidation Using IMS and Molecular Dynamics

J. Phys. Chem. A, Vol. 113, No. 29, 2009 **8225**

Figure 3. Arrival time distributions (ATD) of BK 1-5 [M + H]$^+$ ions as a function of the IM field strength/pressure ratio (E/p = 10−40 V cm^{-1} Torr^{-1}). Note the variation from a near 3-component distribution to a mainly 1-componet distribution as E/p increases.

experimental conditions, the effective ion temperature (T_{eff}) is a function of E/p, and the ions possess a relatively narrow distribution of internal energies.[72] IMS separations can be described as either low- or high- field separations depending on the E/p ratios,[22] i.e., depending upon the amount of translational energy (E_k) obtained by the ion between collisions. That is, under low-field conditions ($T_{eff} \sim T_{BG}$) the ion gains very little E_k and the extent of collisional activation is minimal, whereas under high-field conditions ($T_{eff} > T_{BG}$) the ions can undergo significant amounts of collisional activation. IMS separation of peptide ions above low-field conditions can lead to equilibration among peptide ion conformers, and the E/p ratios at which such equilibration occurs have a strong dependence on the size and nature of the peptide ion.[37,73] Moreover, at high-field conditions the extent of collisional activation may be sufficient to result in the parent ion fragmentation (collision induced dissociation, CID).[74−80]

The effective ion temperature T_{eff} is a function of the type of ion-neutral interaction for a given E/p and T_{BG}. The E/p values may change along the IM cell axis because of the electrode geometry. Although uniform IM cells provide the easiest way of establishing a continuous E/p value near the IM cell axis, we have previously shown the advantages in ion transmission of the periodic IM cell design,[41,81] specifically the variation of ion kinetic energy and ion velocity components along a IM cell axis as a function of E/p for BK1-5 peptide ion (m/z 574 and CCS 170 Å^2) are shown in Figure 2. The electrode spacing and voltage drop create a periodic high-low field strength config-uration, where ions experience periodic accelerating/decelerating cycles.[82] Close inspection of Figure 2 plots shows that the velocity component parallel to the electric field is directly related to the high-low electric field configuration and defines the drift time, whereas the orthogonal velocity components are much

smaller and mainly contribute to the ion diffusion. The ion dynamics information using the EHSS model can be correlated with the effective ion temperature ($T_{eff}^{elastic} = T'_{eff}(\xi \rightarrow 0)$) using eq 4. As E/p increases from 10 to 40 V cm^{-1} Torr^{-1}, the $T_{eff}^{elastic}$ increases from 318 to 500 K (see Table 1). The random nature of the ion−neutral collision changes the ion path inside the cell (i.e., ions experience different electric field gradients) and produces a broader distribution of the $T_{eff}^{elastic}$ along the IM cell axis (up to 50 K), even for a constant E/p and T_{BG} value. Numerical calculations have shown that in most practical cases α' and β' are substantially less than 0.1 (see eq 2),[54] so the accuracy obtained by setting them equal to zero (which is simply the first approximation of the two-temperature theory) is generally good, as illustrated by comparing the $T_{eff}^{elastic}$ values for $\beta' = 0$ and 0.1 in Table 1. Since the ion structure is defined by the thermodynamics of the IM experiment, the overall result is that the IM measured drift time is an average over all the transient conformations the ion experiences as it traverses the IM cell. That is, transient conformations are determined by the number of accessible structures that coexist inside the IM cell.

Figure 3 contains the arrival time distribution (ATD) of a BK 1-5 [M + H]$^+$ ion as a function of E/p and at constant T_{BG} = 300 K. As the E/p increases from 10 to 40 V cm^{-1} Torr^{-1}, the ATD changes from a near 3-component distribution to mainly a 1-component distribution. To further understand the gas-phase ion structure interconversion process during the IMS experiment, the number of accessible conformations of the BK 1-5 [M + H]$^+$ ion as a function of the effective ion temperatures are theoretically examined below.

An accurate description of the gas-phase conformational space of a peptide ion involves the technical challenge of generating all the thermodynamically accessible structures that correspond to a certain experimental condition, which in our case is defined
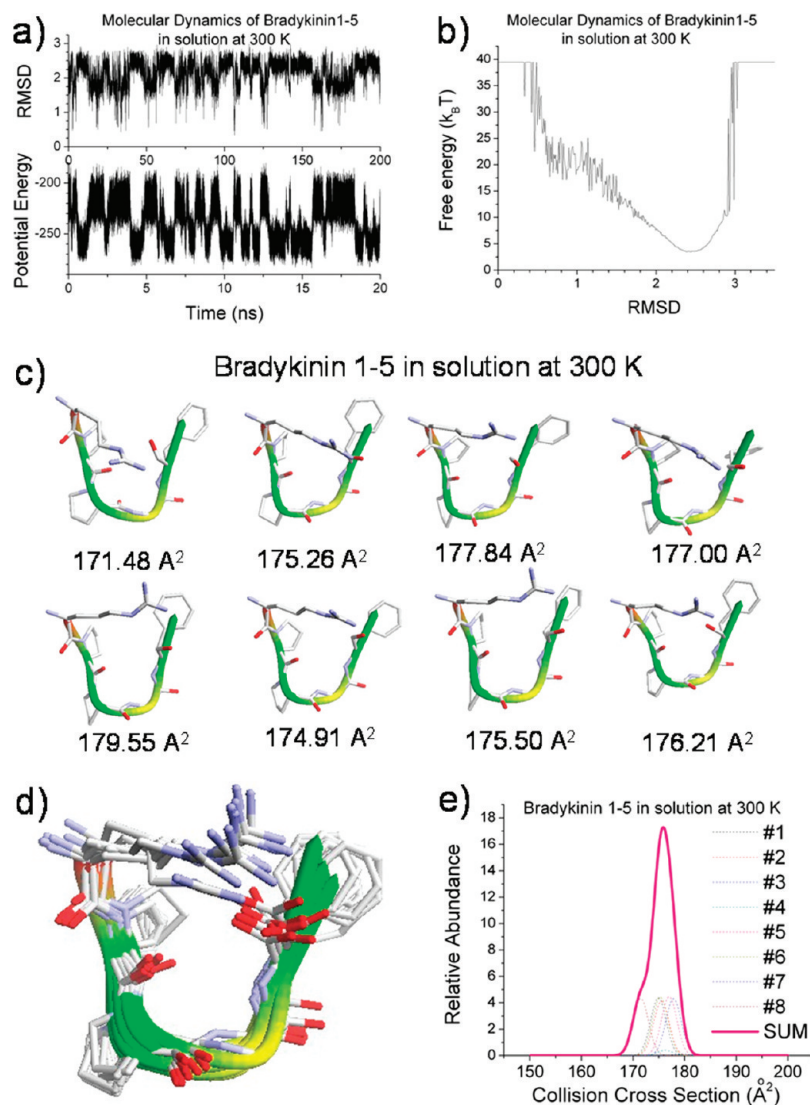
Figure 4. Method B strategy for the analysis of the BK 1-5 peptide in solution at 300 K. (a) Evolution of the RMSD (relative to the starting structure) and potential energy as a function of the MD simulation time. (b) Free energy profile as a function of the RMSD values, where the {structures} vector is obtained from the free energy minima. (c), (d) {CM, %, CCS} vector components and overlay structures obtained after the CA. (e) Expected theoretical CCS profile from the solution {CM, %, CCS} vector in an equivalent IMS experiment at 300 K of helium bath gas.

by the effective ion temperature of the IMS experiments. A major difficulty in simulating processes occurring in IMS experiments is the long time scale (typically hundreds of microseconds) available to the molecular ion for structural rearrangements, whereas standard MD simulations are typically limited to tens of nanoseconds.[26] Two methods are described to overcome this limitation: (i) a simulated annealing MD−CA−constant temperature MD−CA (Method A) and (ii) a generalized non-Boltzmann sampling MD−free energy analysis−CA (Method B). Both methods are meant to generate a conformational space described by a {structure} vector, which is further used to create the theoretical IMS profile as a function of the effective ion temperature. Method A takes advantage of the {≠structures} identity vector as an input for the MD, which increases the probability of generating input structures closely related to the most stable conformers as a function of the effective ion temperature. On the other hand, Method B allows configurations of the system to be sampled in a wide energy range by using an enhanced sampling method.[26]

Figure 4a contains the evolution of the potential energy (E_{pot}) and RMSD as a function of the MD simulation time for the

BK1-5 solution-phase structures obtained using Method B. The advantages of Method B for solution based conditions have been previously reported.[25,26,62] A good correspondence is observed between the variation of E_{pot} and the RMSD over time, which means that the conformational interconversion barriers are being overcome several times in one MD simulation.[26] The obtained structures were classified by their RMSD and free energy values (Figure 4b) and the lower free energy structures were stored in the {structure} vector with ∼3000 components. The CA of the {structure} vector generated eight center-of-mass (CM) structures (Figure 4c); these structures differ in the orientation of the side chains (see overlay structures in Figure 4d). Overall, the BK 1-5 most stable solution-phase structures are characterized by a U-shape, stabilized by a charge interaction between the positively charged N-terminus and arginine residue with the negatively charged C-terminus. This U-shape geometry is also stabilized by a trans−trans conformation at the proline−proline residues.

The generation of different gas-phase ionic forms of biologically relevant molecules has been previously observed,[83−85] and in our hypothesis the existence of either form strongly depends
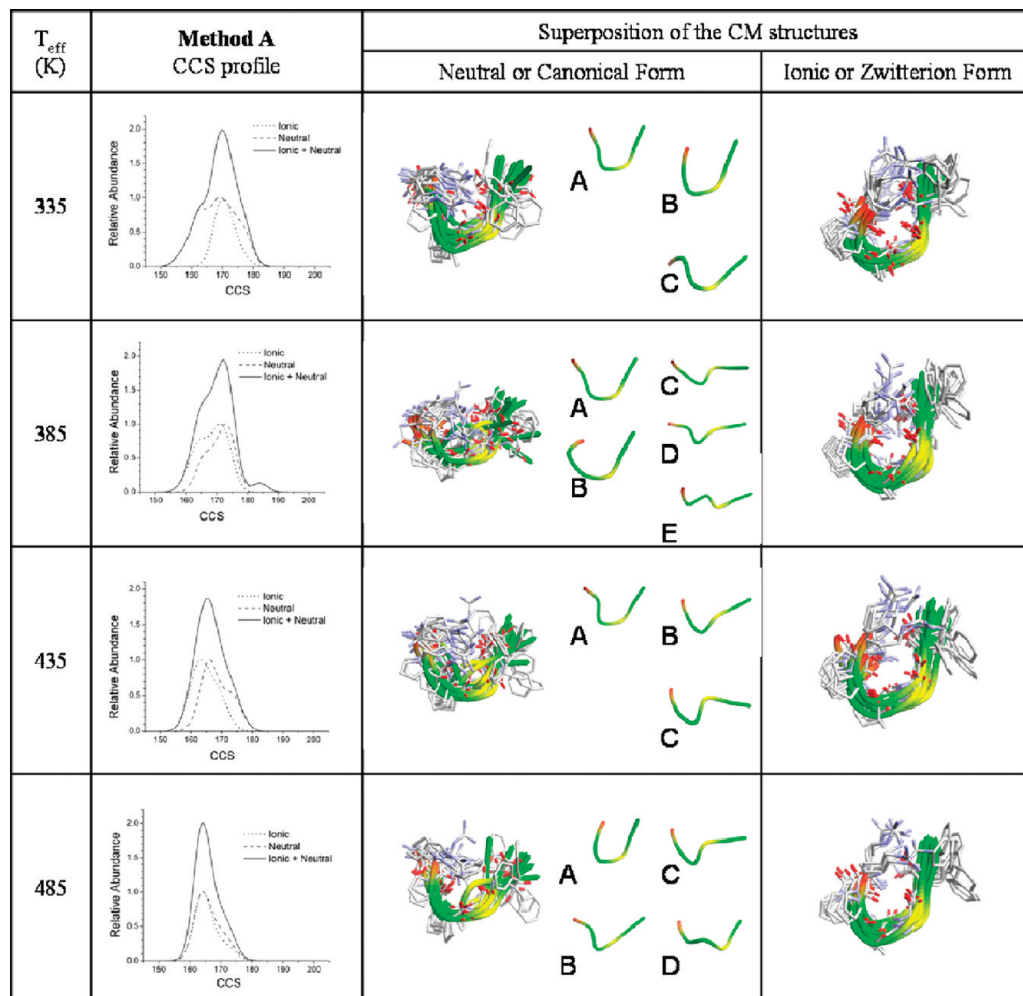
Figure 5. Collision cross-section profile obtained from the {CM, %, CCS} vector for the BK 1-5 $[M + H]^+$ ion as a function of the effective ion temperature using Method A. The CM structures are overlay in the right columns, and the different backbone classes of the neutral or canonical form are illustrated.

on the solution conditions and ionization source. Although complementary H/D exchange experiments have been performed for the BK 1-5 $[M + H]^+$ ion, the results did not exclude the existence of any form.[37] That is, previous H/D exchange results were used to support the assignment of multiple conformers, but the data were not used to infer structural preference. Consequently, we choose two initial gas-phase conformers: (i) a neutral or canonical form (e.g., NH_2-RPPGF-COOH) and (ii) an ionic or zwitterionic form (e.g., NH_3^+-RPPGF-COO⁻).[83−85]

Theoretical CCS profiles and CM structures for BK 1-5 $[M + H]^+$ ions as a function of the effective ion temperature obtained using Methods A and B are contained in Figures 5 and 6, respectively. Inspection of Figures 5 and 6 shows that the theoretical ionic + neutral CCS distribution follows the same trend as that observed when the E/p values are increased in the IMS experiments (Figure 3), independent of the method used; i.e., T_{eff} increases as E/p increases, and the ATD profile changes from a 3-component to mainly a 1-component distribution. In addition, the fact that the theoretical neutral CCS distribution also follows the same trend is consistent with our hypothesis that the preferred conformation has a strong dependence on the solution conditions (i.e., starting solvent systems varying percents of water/methanol), in good agreement with previously reported experimental results.[37] That is, the observation of a 1- or 3-component ATD distribution depends on the BK1-5 solution conditions, which defines the relative abundance of

canonical and zwitterionic form ions: a pure or zwitterionic form of BK 1-5 $[M + H]^+$ ions will mainly generate a 1-component ATD distribution (independent of T_{eff}), whereas a pure canonical form of BK 1-5 $[M + H]^+$ ions will mainly generate a 3-component ATD distribution (at $T_{eff} < 400$ K).

Relative abundance of BK 1-5 $[M + H]^+$ canonical and zwitterionic form ions obtained using Methods A and B as a function of the effective ion temperature are contained in Tables 2−5 and Figures 5 and 6. Comparison of the {CM, %, CCS} vectors obtained from Methods A and B shows that both methods generate similar CCS distributions; however, a greater number of components are found in the vector produced by Method A. Method B generates a {CM, %, CCS} vector that only contains structures that correspond to free energy minima which are the most abundant structures generated by Method A. The main difference between the Methods A and B consists in that free energy analysis cannot be performed by Method A because the {CM, %, CCS} vector is obtained from independent trajectory simulations. Nevertheless, the use of Method A is of interest as a control experiment for the optimization of Method B. As the number of amino acids in the peptide increases, the conformational diversity increases, and this effect is evidenced by the number of multiple MD simulations necessary to be performed at a given effective ion temperature using Method A to reproduce the CCS profile. Moreover, this effect is more feasible to overcome in Method B since the total conformational
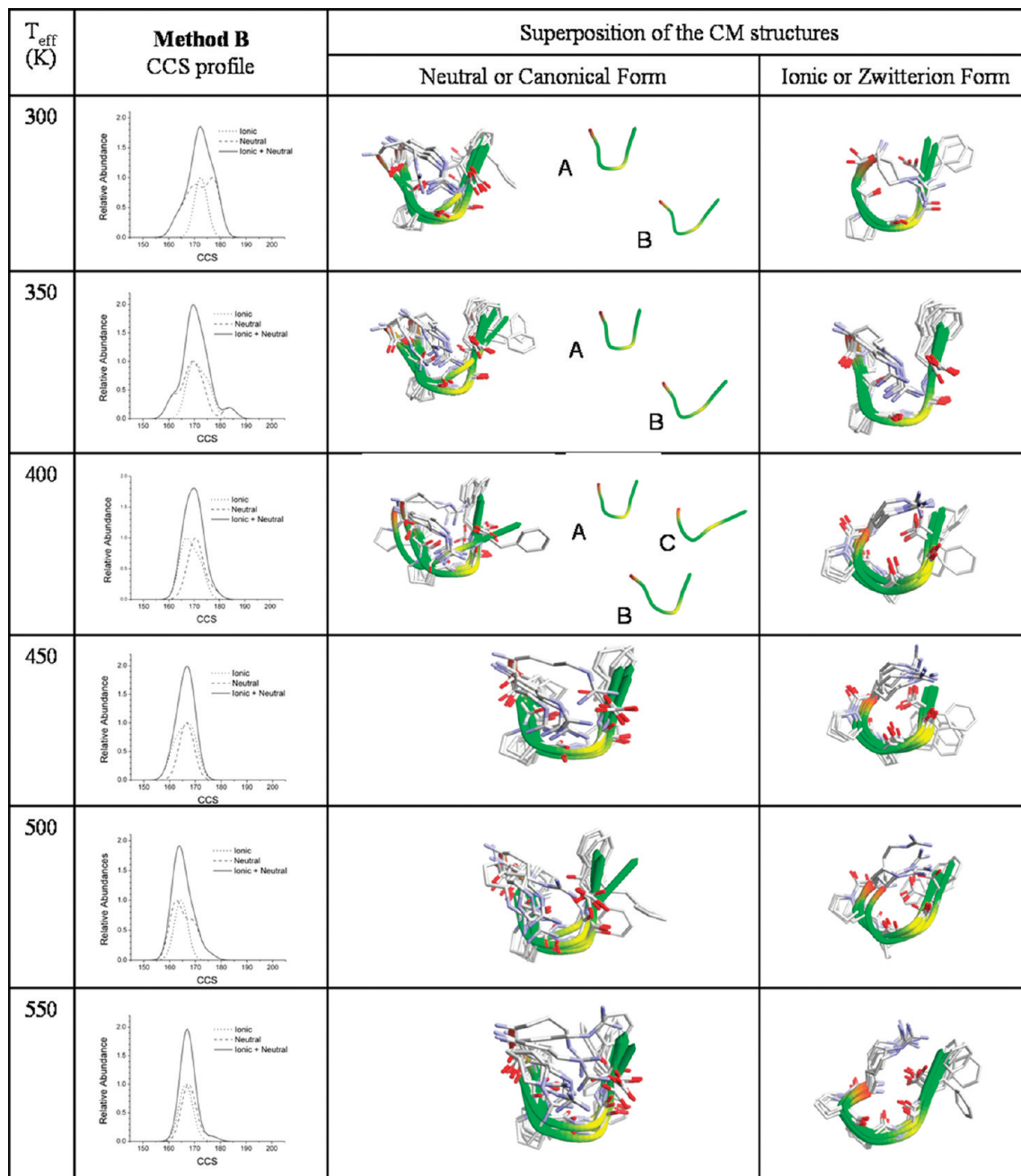
Figure 6. Collision cross-section profile obtained from the {CM, %, CCS} vector for the BK 1-5 [M + H]$^+$ ion as a function of the effective ion temperature using Method B. The CM structures are overlay in the right columns, and the different backbone classes of the neutral or canonical form are illustrated.

space is filtered by the free energy values, and the analysis is performed on the {structures} vector that contain only the lower free energy structures, thus limiting the search to potential candidate structures of interest rather than to the total conformational space. The main advantages of Method B over Method A are (i) single MD in contrast to multiple MD simulations and (ii) availability of thermodynamic information.

Inspection of the zwitterionic BK 1-5 [M + H]$^+$ ion shows that, regardless of the effective ion temperature, all the representative structures show the same backbone configuration. This effect is illustrated in Figures 5 and 6, where the representative structures are overlaid on the backbone RMSD. Differences are observed for the orientation of the phenylalanine residue, whereas a charge interaction between the positively charged N-terminus and arginine residue with the negatively charged C-terminus defines a U-shape structure, similar to that

observed in solution-phase simulations. Results obtained using Method A show that the proline−proline configuration may occur in a large diversity of modes (Table 3); however, small differences are observed in the total conformational space as depicted in the overlaid structures shown in Figure 5. Different conformations that arise from populations of cis and trans forms of proline have been previously observed in IM experiments.[86] Analysis of the BK 1-5 [M + H]$^+$ ion lower free energy structures (Method B) shows that the proline−proline configuration changes from a trans−trans to a cis−cis mode as the T_{eff} increases (Table 5). Overall, the contribution of the proline−proline orientation to the CCS values is small compared to the charge interaction and the arginine and phenylalanine residues orientation because of the small size of the BK 1-5 [M + H]$^+$ ion (Figure 6).

Structure Elucidation Using IMS and Molecular Dynamics

J. Phys. Chem. A, Vol. 113, No. 29, 2009 **8229**

TABLE 2: Components of the {CM, %, CCS} Vector Obtained Using Method A for the Neutral or Canonical Form (e.g., NH$_2$-RPPGF-COOH) of the BK 1-5 [M + H]$^+$ Ion[a]

structure	backbone class and P−P mode		%	CCS (Å^2)	structure	backbone class and P−P mode		%	CCS (Å^2)
	$T_{\text{eff}} = 335 \pm 50$ K					$T_{\text{eff}} = 385 \pm 50$ K			
125_0	A 88%	trans−trans	6.79	157	274_1	A 64%	trans−trans	9.65	164
144_6			15.06	161	156_2			5.04	165
431_1			15.64	167	81_6			2.38	167
42_5			2.82	177	49_3			6.31	167
305_3			7.33	176	176_5			14.87	173
234_4			14.31	172	302_6			4.38	167
308_4			4.49	177	316_5			17.14	175
421_2			10.05	168	143_3		cis−trans	4.12	164
225_5		cis−trans	9.61	162	484_3	B 11%	cis−trans	3.30	164
381_3			2.40	178	258_4		trans−trans	8.21	172
380_0	B 6%	trans−cis	3.03	164	16_2	C 15%	trans−trans	15.44	171
63_5			2.67	169	490_4	D 6%	trans−trans	6.33	183
46_3	C 6%	trans−trans	5.81	172	380_6	E 4%	trans−trans	2.85	170
	$T_{\text{eff}} = 435 \pm 50$ K					$T_{\text{eff}} = 485 \pm 50$ K			
40_1	A 88%	trans−trans	2.40	165	160_1	A 73%	trans−trans	18.01	164
442_1			10.47	168	397_3			4.00	163
64_2			7.01	165	479_4			17.52	168
446_3			3.59	161	113_5			10.78	164
21_4			14.42	165	56_6			17.62	162
56_5			7.96	167	447_5		trans−cis	2.68	161
120_5			10.29	173	171_2			2.51	174
56_6			3.46	165	261_2	B 14%	trans−trans	13.77	171
46_6			2.28	166	339_3	C 3%	trans−cis	2.34	170
100_3		cis−trans	4.97	176	167_3	D 10%	trans−trans	10.76	163
264_3			7.37	170					
140_1			4.38	164					
192_6		trans−cis	6.44	165					
434_4			3.50	163					
465_2	B 9%	trans−cis	8.96	173					
394_6	C 3%	trans−cis	2.51	172					

[a] Vector components were classified by the backbone class (alphabetically, e.g., A, B, C, etc.) and by the proline−proline configuration (P−P mode) of the backbone.

Close inspection of the canonical form of BK 1-5 [M + H]$^+$ ion structures shows a large diversity of backbone configurations, which are probably a consequence of a weaker charge interaction between the N- and C-terminus. The backbone structures were grouped in classes (denoted alphabetically, e.g., A, B, C, etc.), and the percentage of backbone classes are contained in Tables 2 and 4. As the T_{eff} increases, the lower free energy structures are mainly stabilized in a U-shaped backbone configuration (label A), whereas at lower T_{eff} ($T_{\text{eff}} <$ 400 K) the backbone configurations of more elongated forms (label B to E) are observed (see Table 4 and Figure 6). The contribution of A structures to the total conformational space (Method A results in Table 2) peaks at 36% (at $T_{\text{eff}} = 385$ K), and if filtered by the lower free energy structures (Method B results in Table 4), their contribution peaks at 18% (at $T_{\text{eff}} =$ 350 K). That is, both Methods A and B suggest that the larger backbone diversity is observed at T_{eff} values that corresponds to the broader 3-component ATD distribution observed in the IMS experiments (Figure 3). It is important to note that in the case of Method A, despite the large number of MD simulations performed, the abundance analysis may be in error because the comparison is made between independent trajectories, making it difficult to correlate the most abundant structures with the lower free energy structures. The lower free energy structures (Method B) are mainly characterized by a trans−trans mode of the proline−proline configuration of the backbone (Table 4), equivalent to that observed in solution (Figure 4), regardless of the T_{eff}. Results obtained using Method A show that the other proline−proline configuration occurs in a lower abundance (Table 2), and probably at higher free energy values, which

makes them less probable to be experimentally observed. Although the more elongated forms will contribute to a broader CCS distribution, the orientation of the arginine and phenylalanine residues may mask this effect owing to the small size of the BK 1-5 [M + H]$^+$ ion.

Figure 7 contains the experimental ATDs, theoretical CCS profile and candidate structure for BK1-8 (RPPGFSPF) [M + H]$^+$ ions. Inspection of Figure 7a shows that the BK1-8 ATD distributions are best described as broad single-component peak, independent of the E/p values. The broad ATD distribution may be attributed to multiple gas-phase peptide ion conformations (labeled A, B, C, and D by their backbone configuration in Figure 7c) that coexist as a function of T_{eff}. The candidates' structures were obtained using Method B as a function of T_{eff}. Note that, as T_{eff} increases, a number of conformations are observed for both the zwitterionic and canonical forms, and the relative abundances are contained in Table 6. The data contained in Table 6, specifically the relative abundances of each candidate structure, suggests that they can be grouped according to their backbone configuration, labeled A, B, C, and D in Figure 7c (all structures are shown in the Supporting Information). Although a small number of backbone orientations are obtained, the orientation of side chain groups relative to the backbone increases the available conformational space for the BK1-8 peptide ions, which is reflected in the broad CCS distribution profiles observed in Figure 7b. In addition, the configuration (trans−trans−trans or trans−trans−cis) of the proline amino acids in positions P$_2$, P$_3$, and P$_7$ of BK1-8 will also increase the structural diversity, i.e., CCS distribution. Although a U-shape of the backbone is conserved (between the N- and C- terminus

TABLE 3: Components of the {CM, %, CCS} Vector Obtained Using Method A for the Ionic or Zwitterionic Form (e.g., NH_3^+-RPPGF-COO^-) of the BK 1-5 $[M + H]^+$ Ion[a]

structure	%	P−P mode	CCS ($Å^2$)	structure	%	P−P mode	CCS ($Å^2$)
T_{eff} = 335 ± 50 K				T_{eff} = 385 ± 50 K			
160_3	3.20	trans−trans 32%	173	157_2	2.19	trans−cis 45%	163
424_6	16.78		169	149_3	7.68		172
116_3	11.59		169	33_3	9.12		170
112_1	2.50	trans−cis 15%	171	94_4	1.77		169
305_1	4.77		174	161_4	14.90		170
136_2	1.83		177	294_6	5.63		162
397_3	2.11		174	358_6	4.34		164
120_5	3.91		177	425_1	4.17	cis−trans 40%	165
44_0	4.53	cis−trans 29%	174	410_2	3.55		159
367_2	8.61		172	450_4	2.98		167
258_4	15.65		169	353_4	13.60		173
32_1	2.33	cis−cis 24%	173	216_5	12.08		165
387_1	6.21		167	207_4	3.25		164
248_2	3.86		168	218_2	6.35	cis−cis 15%	167
212_5	2.13		170	369_3	4.31		163
418_5	10.00		171	207_6	4.07		162
T_{eff} = 435 ± 50 K				T_{eff} = 485 ± 50 K			
49_2	2.86	trans−cis 15%	160	500_2	8.98	trans−cis 12%	169
195_2	6.88		171	52_6	2.99		164
28_4	5.96		158	163_3	15.33	cis−trans 72%	163
71_1	13.99	cis−trans 63%	162	350_4	4.07		173
129_1	5.89		168	413_5	19.71		163
454_2	3.09		170	459_6	13.91		164
440_3	3.99		173	396_1	19.24		166
488_4	11.06		161	125_6	2.38	cis−cis 16%	168
438_5	6.49		169	178_2	3.52		161
248_6	18.26		166	234_2	5.82		172
70_6	3.97	cis−cis 22%	169	357_3	4.03		163
49_3	13.92		163				
275_4	3.65		162				

[a] Vector components were classified by the proline−proline configuration (P−P mode) of the backbone.

TABLE 4: Components of the {CM, %, CCS} Vector Containing the Lower Free Energy Structures Obtained Using Method B for the Neutral or Canonical Form (e.g., NH_2-RPPGF-COOH) of the BK 1-5 $[M + H]^+$ Ion[a]

structure	backbone class and P−P mode		20.87	CCS ($Å^2$)	structure	backbone class and P−P mode		19.19	CCS ($Å^2$)
T_{eff} = 300 K					T_{eff} = 350 K				
404_1	A 94%	trans−trans	20.87	167	275_1	A 82%	trans−trans	19.19	161
327_2			20.97	178	245_2			18.88	172
10_3			21.17	176	475_3			19.06	169
80_4			18.28	171	187_5			6.56	167
210_1			12.30	163	335_4			18.44	167
103_5	B 6%	trans−trans	6.42	171	414_2	B 18%	trans−trans	9.55	183
					339_1			8.32	173
T_{eff} = 400 K					T_{eff} = 450 K				
76_1	A 86%	trans−trans	22.42	170	299_1	A 100%	trans−trans	15.74	168
422_3			24.45	167	464_2			13.89	167
116_4			14.54	171	164_2			22.28	164
98_2			24.45	171	274_3			16.12	165
154_1	B 6%	trans−trans	6.20	175	389_4			16.23	168
13_1	C 8%	trans−cis	7.94	178	299_5			15.74	166
T_{eff} = 500 K					T_{eff} = 550 K				
228_1	A 100%	trans−trans	16.62	164	446_1	A 100%	trans−trans	18.30	170
72_2			15.37	169	205_2			15.75	166
301_2			20.62	162	60_2			7.00	166
144_3			17.10	169	273_3			7.00	166
90_4			16.26	161	403_3			9.29	166
242_4			6.07	175	235_4			7.87	166
1_5			7.97	161	56_4			19.52	167
					10_5			22.7	165

[a] Vector components were classified by the backbone class (alphabetically, e.g., A, B, C, etc.) and by the proline−proline configuration (P−P mode) of the backbone.

orientations), the larger number of amino acids in the BK1-8 peptide leads to a larger structural diversity in the center part of the backbone. Close inspection of Table 6 shows that most of the lower free energy structures are stabilized in a trans−trans−trans mode, and only some components of the canonical form at T_{eff} = 400 are stabilized in the trans−trans−cis

TABLE 5: Components of the {CM, %, CCS} Vector Containing the Lower Free Energy Structures Obtained Using Method B for the Ionic or Zwitterionic Form (e.g., NH_3^+-RPPGF-COO^-) of the BK 1-5 $[M + H]^+$ Ion[a]

structure	%	P–P mode	CCS ($Å^2$)	structure	%	P–P mode	CCS ($Å^2$)
		T_{eff} = 300 K				T_{eff} = 350 K	
296_1	53.07	trans–trans 100%	171	369_1	20.38	trans–trans 66%	170
276_2	46.93		172	399_2	18.49		175
				216_3	21.32		173
				31_4	6.59		168
				290_4	14.87	cis–cis 34%	169
				35_5	18.34		168
		T_{eff} = 400 K				T_{eff} = 450 K	
22_1	27.65	cis–cis 100%	172	101_1	19.83	cis–cis 100%	161
467_2	26.15		165	231_2	18.30		168
31_3	32.08		167	48_2	6.23		171
463_3	14.12		170	455_3	24.19		164
				211_4	22.95		168
				64_5	8.50		165
		T_{eff} = 500 K				T_{eff} = 550 K	
399_1	25.44	cis–cis 100%	164	243_1	18.59	cis–cis 100%	164
478_2	27.49		163	457_2	18.80		166
137_2	22.11		164	204_3	18.85		166
191_3	24.97		164	218_4	18.46		167
				68_5	18.94		166
				170_6	6.37		170

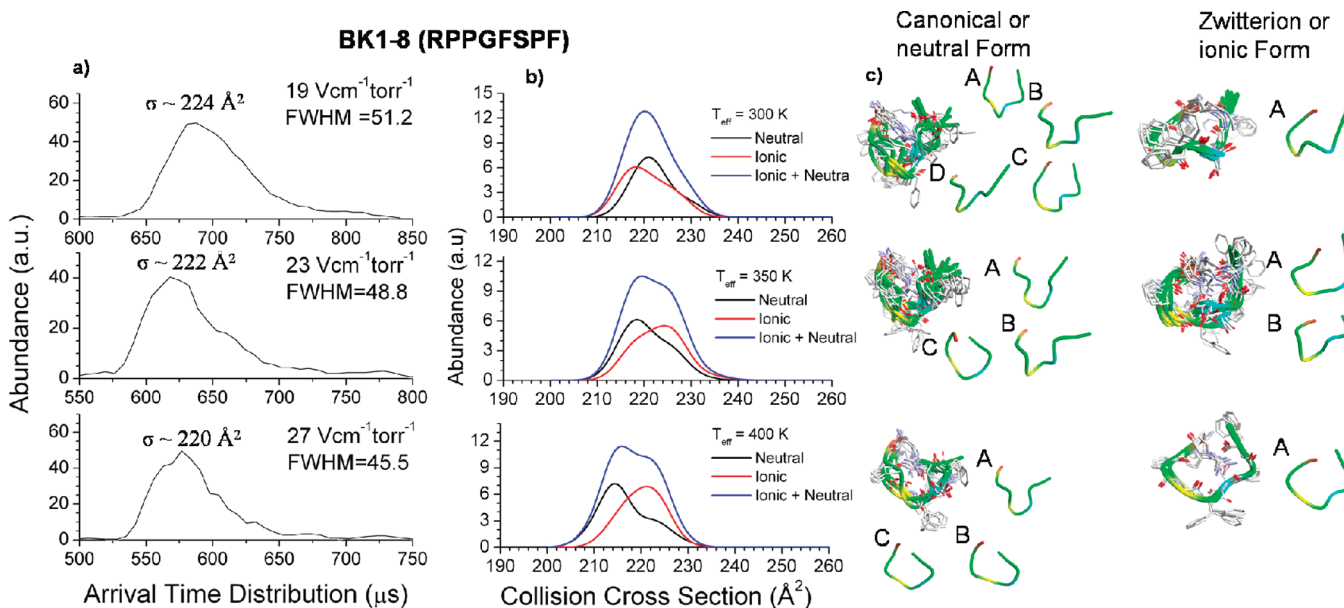[a] Vector components were classified by the proline–proline configuration (P–P mode) of the backbone.

Figure 7. (a) Arrival time distribution (ATD) of BK1-8 $[M + H]^+$ ions as a function of the IM field strength/ pressure ratio (E/p = 19, 23, and 27 V cm^{-1} $Torr^{-1}$). (b) BK1-8 collision cross-section profile obtained from the {CM, %, CCS} vector as a function of the ion effective temperature (T_{eff} = 300, 350, and 350 K) using Method B. (c) Overlay and representative backbone structures (labeled as A–D in each case) of the canonical (or neutral) and zwitterionic (or ionic) forms are illustrated. (All structures are contained in the Supporting Information).

mode. A smaller number of backbone orientations is observed for the BK1-8 zwitterionic or ionic form (Figure 7c), which may be related to a higher stabilization provided by interaction of the charged groups of the N-terminus, the guanidine group of the arginine (R_1 position), and the C-terminus, whereas such interactions are weaker for the BK1-8 canonical or neutral form. A good agreement is observed between the experimental (ATD profile) and the theoretical (CCS profile) results for the ionic + neutral distribution, which suggest that BK1-8 $[M + H]^+$ ions can exist as either canonical or zwitterionic forms in the gas phase.

Conclusions

The ion dynamic simulations showed that under low-field conditions ($T_{eff} \sim T_{BG}$) the ion gains very little translational energy and the extent of collisional activation is minimal, whereas above the low-field conditions ($T_{eff} > T_{BG}$) the ions may be collisionally activated and conformational barriers may be overcome. Two methods were described to efficiently sample the gas-phase conformational space of molecular ions as a function of the T_{eff} characteristic of the IMS experiments. The T_{eff} description shows that an unambiguous determination of rearrangement reactions requires a high separation in the IM domain and the verification of the primary structure by performing CID on the multiple conformations as they exit the IM cell. The observation of multiple conformations in the IM domain demands (i) the existence of conformational barriers at T_{eff} and (ii) a difference between multiple conformations larger than the ion diffusion contribution.

TABLE 6: Components of the {CM, %, CCS} Vector Containing the Lowest Free Energy Structures Obtained Using Method B for the Canonical (or Neutral) and Zwitterionic (or Ionic) Form of the BK1-8 [M + H]$^+$ Ion^a

BK1-8 canonic or neutral from				BK1-8 zwitterionic or ionic form			
structure	%	P−P−P mode	CCS (Å^2)	structure	%	P−P−P mode	CCS (Å^2)
T_{eff} = 300							
8_1	4.6	trans−trans−trans	220	339_1	21.2	trans−trans−trans	218
58_1	12.6		229	393_1	0.6		214
217_1	3.5		226	553_1	21.5		216
249_1	0.3		243	1414_3	21.2		222
270_1	0.3		223	1631_4	0.6		231
925_2	22.5		218	1668_4	18.7		227
995_2	0.3		219				
1158_3	23		221				
1643_4	17		222				
T_{eff} = 350							
166_1	12.5	trans−trans−trans	218	266_1	0.6	trans−trans−trans	235
308_1	0.4		226	295_1	19.1		217
428_1	3.1		214	482_1	0.8		222
636_2	7.1		216	599_2	17.9		221
713_2	7.8		225	723_2	2.1		234
975_2	0.7		223	988_2	0.5		238
1034_3	2.4		230	1139_3	20.4		225
1214_3	6.7		226	1648_4	0.4		225
385_1	15.7		218	1705_4	15.9		227
649_1	5.9		215	1916_4	2.7		230
788_2	1.1		233				
850_2	7.9		226				
1334_3	11.0		220				
T_{eff} = 400							
304_1	9.1	trans−trans−cis	209	123_1	28.1	trans−trans−trans	218
464_1	5.0		228	862_2	23.8		224
529_2	3.6		222	1133_3	21.5		222
720_2	25.4		215	1428_3	2.3		228
848_2	2.2		219	1563_4	13.3		214
1054_3	30.0		214				
125_1	17.2	trans−trans−trans	223				

^{a} Backbone orientations of the proline positions P$_2$, P$_3$, and P$_7$ are classified in trans or cis modes.

Two methods are described to generate a conformational space describe by a {structure} vector, which is further used to create the theoretical {CM, %, CCS} IMS profile as a function of T_{eff}: (i) a simulated annealing MD−CA−constant temperature MD−CA (Method A), and (ii) a generalized non-Boltzmann sampling MD−free energy analysis−CA (Method B). Method A proved to be useful to generate the total conformational space, while Method B has advantages in requiring a shorter computational time in providing thermodynamic information, thus enabling by filtering the free energy values a more efficient characterization of the conformational space accessible to a given ion as a function of T_{eff}.

In the case of the BK 1-5 [M + H]$^+$ peptide ion, the description of the conformational changes as a function of T_{eff} showed that, as T_{eff} increases, the conformational space changes from a 3-component distribution to mainly a 1-component distribution, in good agreement with the experimental observations. Close inspection of the representative structures showed that the secondary structure of a BK 1-5 [M + H]$^+$ ion can exist in the canonical and/or zwitterionic form in the gas phase, where the relative abundances of the canonical and zwitterionic forms are defined by the percent of water/methanol in the starting solution. Analysis of the zwitterionic form BK 1-5 [M + H]$^+$ ions showed that, independent of the T_{eff}, all the representative structures are stabilized in a U-shape backbone configuration, similar to that observed in solution-phase conditions. On the other hand, the canonical form of BK 1-5 [M + H]$^+$ ions showed a large diversity of backbone configurations

that depend on the T_{eff}: as T_{eff} increases, the lower free energy structures are mainly stabilized in a U-shaped backbone configuration, whereas at lower T_{eff} values (T_{eff} < 400 K) the backbone configurations of more elongated forms are also observed. This structural diversity of the canonical form of the BK 1-5 [M + H]$^+$ ions is probably a consequence of a weaker charge interaction between the N- and C-terminus. The theoretical analysis of Bradykinin peptide BK1-8 [M + H]$^+$ ions showed that the conformational space can be described by a broad single-component distribution independent of T_{eff}, in good agreement with the experimental observations. Analogous to the BK1-5, these results suggest that the BK1-8 [M + H]$^+$ ions can exist in the canonical or zwitterionic forms in the gas phase. A larger number of backbone orientations is observed for the canonical or neutral form of the BK1-8 [M + H]$^+$ ions, whereas a smaller number is observed for the zwitterionic or ionic form as a result of the charge interaction between the N-terminus, guanidine group of the arginine (R$_1$ position) and the C-terminus provides. Although a U-shape of the backbone is still conserved (between the N- and C- terminus orientations), the larger number of amino acids in BK1-8 peptide leads to a larger structural diversity in the central part of the backbone.

Overall, the new approach provides a higher statistical confidence in the gas-phase structure classification and/or identification when compared with the experimental IM determined ion-neutral, collision cross sections. This work provides a step forward, providing IMS data with theoretical tools for understanding the mechanism of molecular ion rearrangements

Structure Elucidation Using IMS and Molecular Dynamics

J. Phys. Chem. A, Vol. 113, No. 29, 2009 **8233**

under controlled experimental conditions. After further validation of this method with larger protein and protein aggregate systems, our approach has the potential to contribute significantly to the understanding of the key elements that define the number of conformational isomers and the folding mechanism of peptide and protein ions in the gas phase.

Supporting Information Available: Backbone orientations of the lowest free energy structures obtained using a generalized non-Boltzmann sampling MD−free energy analysis−CA (Method B) for the canonical (or neutral) and zwitterionic (or ionic) form of BK1-8 peptide, RPPGFSPF, $[M + H]^+$. This material is available free of charge via the Internet at http://pubs.acs.org.

References and Notes

(1) Karp, D. A.; Gittis, A. G.; Stahley, M. R.; Fitch, C. A.; Stites, W. E.; Garcia-Moreno E, B *Biophys. J.* **2007**, *92*, 2041.

(2) Fitch, C. A.; Whitten, S. T.; Hilser, V. J.; García-Moreno E., B. *Proteins: Struct., Funct., Bioinformatics* **2006**, *63*, 113.

(3) Bone, S. *J. Bioelectricity* **1985**, *4*, 389.

(4) Wang, Y.; Zhang, H.; Li, W.; Scott, R. A. *Proc. Natl. Acad. Sci. U.S.A.* **1995**, *92*, 709.

(5) Weiss, W. F. I. V.; Hodgdon, T. K.; Kaler, E. W.; Lenhoff, A. M.; Roberts, C. J. *Biophys. J.* **2007**, *93*, 4392.

(6) Karas, M.; Bachmann, D.; Hillenkamp, F. *Anal. Chem.* **1985**, *57*, 2935.

(7) Hillenkamp, F.; Karas, M. *Int. J. Mass Spectrom.* **2000**, *200*, 71.

(8) Whitehouse, C. M.; Dreyer, R. N.; Yamashita, M.; Fenn, J. B. *Anal. Chem.* **1985**, *57*, 675.

(9) Cole, R. B. *Electrospray Ionization Mass Spectrometry*; John Wiley & Sons: New York, 1997.

(10) Aebersold, R.; Goodlett, D. R. *Chem. Rev.* **2001**, *101*, 269.

(11) Miranker, A.; Robinson, C. V.; Radford, S. E.; Aplin, R. T.; Dobson, C. M. *Science* **1993**, *262*, 896.

(12) Valentine, S. J.; Clemmer, D. E. *J. Am. Soc. Mass Spectrom.* **2002**, *13*, 506.

(13) Resing, K. A.; Hoofnagle, A. N.; Ahn, N. G. *J. Am. Soc. Mass Spectrom.* **1999**, *10*, 685.

(14) Deng, Y.; Zhang, Z.; Smith, D. L. *J. Am. Soc. Mass Spectrom.* **1999**, *10*, 675.

(15) Nemirovskiy, O.; Giblin, D. E.; Gross, M. L. *J. Am. Soc. Mass Spectrom.* **1999**, *10*, 711.

(16) Figueroa, I. D.; Russell, D. H. *J. Am. Soc. Mass Spectrom.* **1999**, *10*, 719.

(17) Jaime, A. S.; Monia, G.; Oleg, V. B.; Thomas, R. R. *J. Chem. Phys.* **2007**, *127*, 154322.

(18) Hunig, I.; Kleinermanns, K. *Phys. Chem. Chem. Phys.* **2004**, *6*, 2650.

(19) Jarrold, M. F. *Annu. Rev. Phys. Chem.* **2000**, *51*, 179.

(20) Valentine, S. J.; Counterman, A. E.; Clemmer, D. E. *J. Am. Soc. Mass Spectrom.* **1999**, *10*, 1188.

(21) Tao, L.; McLean, J. R.; McLean, J. A.; Russell, D. H. *J. Am. Soc. Mass Spectrom.* **2007**, *18*, 1232.

(22) Ruotolo, B. T.; McLean, J. A.; Gillig, K. J.; Russell, D. H. *J. Am. Soc. Mass Spectrom.* **2005**, *16*, 158.

(23) Kanu, A. B.; Hill Jr, H. H. *Talanta* **2007**, *73*, 692.

(24) Zilch, L. W.; Kaleta, D. T.; Kohtani, M.; Krishnan, R.; Jarrold, M. F. *J. Am. Soc. Mass Spectrom.* **2007**, *18*, 1239.

(25) Gao, Y. Q.; Yang, L. J. *J. Chem. Phys.* **2006**, *125*, 114103.

(26) Gao, Y. Q. *J. Chem. Phys.* **2008**, *128*, 064105.

(27) Gao, Y. Q. *J. Chem. Phys.* **2008**, *128*, 134111.

(28) Bartels, C.; Karplus, M. *J. Phys. Chem. B* **1998**, *102*, 865.

(29) Darve, E.; Pohorille, A. *J. Chem. Phys.* **2001**, *115*, 9169.

(30) Bussi, G.; Laio, A.; Parrinello, M. *Phys. Rev. Lett.* **2006**, *96*, 090601.

(31) Hamelberg, D.; McCammon, J. A. *J. Am. Chem. Soc.* **2005**, *127*, 13778.

(32) Hamelberg, D.; Mongan, J.; McCammon, J. A. *J. Chem. Phys.* **2004**, *120*, 11919.

(33) Berg, B. A.; Neuhaus, T. *Phys. Lett. B* **1991**, *267*, 249.

(34) Mitsutake, A.; Okamoto, Y. *Chem. Phys. Lett.* **2000**, *332*, 131.

(35) Sugita, Y.; Kitao, A.; Okamoto, Y. *J. Chem. Phys.* **2000**, *113*, 6042.

(36) Hansmann, U. H. E. *Chem. Phys. Lett.* **1997**, *281*, 140.

(37) Sawyer, H. A.; Marini, J. T.; Stone, E. G.; Ruotolo, B. T.; Gillig, K. J.; Russell, D. H. *J. Am. Soc. Mass Spectrom.* **2005**, *16*, 893.

(38) Gillig, K. J.; Ruotolo, B.; Stone, E. G.; Russell, D. H.; Fuhrer, K.; Gonin, M.; Schultz, A. *J. Anal. Chem.* **2000**, *72*, 3965.

(39) Stone, E. G.; Gillig, K. J.; Ruotolo, B. T.; Russell, D. H. *Int. J. Mass Spectrom.* **2001**, *212*, 519.

(40) Ruotolo, B. T.; Gillig, K. J.; Stone, E. G.; Russell, D. H.; Fuhrer, K.; Gonin, M.; Schultz, J. A. *Int. J. Mass Spectrom.* **2002**, *219*, 253.

(41) Gillig, K. J.; Ruotolo, B. T.; Stone, E. G.; Russell, D. H. *Int. J. Mass Spectrom.* **2004**, *239*, 43.

(42) McDaniel, E. W.; Mason, E. A. *Mobility and diffusion of ions in gases*; John Wiley and Sons, Inc.: New York, 1973.

(43) Mesleh, M. F.; Hunter, J. M.; Shvartsburg, A. A.; Schatz, G. C.; Jarrold, M. F. *J. Phys. Chem.* **1996**, *100*, 16082.

(44) Shvartsburg, A. A.; Jarrold, M. F. *Chem. Phys. Lett.* **1996**, *261*, 86.

(45) Watts, P.; Wilders, A. *Int. J. Mass Spectrom. Ion Processes* **1992**, *112*, 179.

(46) McDaniel, E. W.; Viehland, L. A. *Phys. Rep.* **1984**, *110*, 333.

(47) Ellis, H. W.; Thackston, M. G.; McDaniel, E. W.; Mason, E. A. *At. Data Nucl Data Tables* **1984**, *31*, 113.

(48) Ellis, H. W.; Pai, R. Y.; McDaniel, E. W.; Mason, E. A.; Viehland, L. A. *At. Data Nucl. Data Tables* **1976**, *17*, 177.

(49) Ellis, H. W.; McDaniel, E. W.; Albritton, D. L.; Viehland, L. A.; Lin, S. L.; Mason, E. A. *At. Data Nucl Data Tables* **1978**, *22*, 179.

(50) Wang Chang, C. S.; Uhlenbeck, G. E.; de Boer, J. Part C. The Heat Conductivity and Viscosity of Polyatomic Gases. In *Studies in Statistical Mechanics*; Uhlenbeck, J. d. B. a. G. E., Ed.; North Holland: Amsterdam, 1964; *Vol. II*, pp 241.

(51) Waldman, L. In *Statistical Mechanics of equilibrium and Non-Equilibrium*; Meixner, J., Ed. North Holland: Amsterdam, 1965.

(52) McDaniel, E. W.; Mason, E. A. *Mobility and diffusion of ions in gases*; John Wiley and Sons, Inc.: New York, 1973.

(53) Viehland, L. A.; Mason, E. A. *Ann. Phys.* **1975**, *91*, 499.

(54) Viehland, L. A.; Mason, E. A. *Ann. Phys.* **1978**, *110*, 287.

(55) *CFD Fluent*; Fluent 6.2.16 ed.; Fluent Inc.: Lebanon, NH.

(56) *Simion 3D*; Scientific Instrument Services, Inc.: Ringoes, NJ.

(57) Anderson, J. B. *J. Chem. Phys.* **2001**, *115*, 4546.

(58) Ding, L.; Sudakov, M.; Kumashiro, S. *Int. J. Mass Spectrom.* **2002**, *221*, 117.

(59) Berendsen, H. J. C.; Postma, J. P. M.; Gunsteren, W. F. v.; DiNola, A.; Haak, J. R. *J. Chem. Phys.* **1984**, *81*, 3684.

(60) Dinur, U.; Hagler, A. T. New Approaches to Empirical Force Fields. In *Reviews in Computational Chemistry*; Lipkowitz, K. B., Boyd, D. B., Eds.; VCH: New York, 1991; *Vol. 2*, pp 99.

(61) *Accelrys Cerius2 manual*, 4.9 ed.; Accelrys Inc.: 2003.

(62) Lijiang, Y.; Michael Patrick, G.; Yi Qin, G. *J. Chem. Phys.* **2007**, *126*, 125102.

(63) Wang, J. M.; Cieplak, P.; Kollman, P. A. *J. Comput. Chem.* **2000**, *21*, 1049.

(64) Frisch, M. J. ; et al. *Gaussian 03*, revision C.02; Gaussian Inc.: Wallingford, CT, 2004.

(65) Bayly, C. I.; Cieplak, P.; Cornell, W. D.; Kollman, P. A. *J. Phys. Chem.* **1993**, *97*, 10269.

(66) Cieplak, P.; Cornell, W. D.; Bayly, C. I.; Kollman, P. A. *J. Comput. Chem.* **1995**, *16*, 1357.

(67) Pigache, A.; Cieplak, P.; Dupradeau, F.-Y. *Automatic and highly reproducible RESP and ESP charge derivation: Application to the development of programs RED and X RED*; 227th National Meeting of the American Chemical Society; American Chemical Society: Washington, DC, 2004.

(68) Case, D. A.; Darden, T. E.; Cheatham, T. E.; Simmerling, C. L.; Wang, J.; Duke, R. E.; Luo, R.; Merz, K. M.; Wang, B.; Pearlman, D. A.; Crowley, M.; Brozell, S.; Tsui, V.; Gohlke, H.; Mongan, J.; Hornak, V.; Cui, G.; Beroza, P.; Schafmeister, C.; Caldwell, J. W.; Ross, W. S.; Kollman, P. A. *AMBER 8*; University of California, San Francisco, CA, 2004.

(69) Smith, J. SUPPOSE; http://structbio.vanderbilt.edu/~jsmith/, 1997.

(70) Cox, T. F.; Cox, M. A. A. *Multidimensional scaling*; CRC Press: London, 1994.

(71) Seo, J.; Shneiderman, B. *IEEE Comput.* **2002**, *35*, 80.

(72) Revercomb, H. E.; Mason, E. A. *Anal. Chem.* **1975**, *47*, 970.

(73) Verbeck, G. F.; Ruotolo, B. T.; Gillig, K. J.; Russell, D. H. *J. Am. Soc. Mass Spectrom.* **2004**, *15*, 1320.

(74) Valentine, S. J.; Koeniger, S. L.; Clemmer, D. E. *Anal. Chem.* **2003**, *75*, 6202.

(75) Koeniger, S. L.; Merenbloom, S. I.; Valentine, S. J.; Jarrold, M. F.; Udseth, H. R.; Smith, R. D.; Clemmer, D. E. *Anal. Chem.* **2006**, *78*, 4161.

(76) Merenbloom, S. I.; Bohrer, B. C.; Koeniger, S. L.; Clemmer, D. E. *Anal. Chem.* **2007**, *79*, 515.

(77) Merenbloom, S. L.; Koeniger, S. L.; Bohrer, B. C.; Valentine, S. J.; Clemmer, D. E. *Anal. Chem.* **2008**, *80*, 1918.

(78) Fernandez-Lima, F. A.; Becker, C.; Gillig, K. J.; Russell, W. K.; Tichy, S. E.; Russell, D. H. *Anal. Chem.* **2009**, *81*, 618.

(79) Fernandez-Lima, F. A.; Becker, C.; Gillig, K.; Russell, W. K.; Nascimento, M. A. C.; Russell, D. H. *J. Phys. Chem. A* **2008**, *112*, 11061.

(80) Becker, C.; Fernandez-Lima, F. A.; Gillig, K. J.; Russell, W. K.; Cologna, S.; Russell, D. H. *J. Am. Soc. Mass Spectrom.* **2009**, *20*, 907.

(81) Gillig, K. J.; Russell, D. H. A periodic field focusing ion mobility spectrometer. *Patent Cooperation Treaty Int. Appl. WO0165589;* The Texas A & M University System: College Station, TX, 2001; p 36.

(82) Fuhrer, K.; Gonin, M.; Schultz, J. A. Ion mobility spectrometer. *U.S. Patent Application Publ. US20050189486*, 2005; p 38.

(83) Strittmatter, E. F.; Lemoff, A. S.; Williams, E. R. *J. Phys. Chem. A* **2000**, *104*, 9793.

(84) Strittmatter, E. F.; Williams, E. R. *J. Phys. Chem. A* **2000**, *104*, 6069.

(85) Jockusch, R. A.; Lemoff, A. S.; Williams, E. R. *J. Am. Chem. Soc.* **2001**, *123*, 12255.

(86) Counterman, A. E.; Clemmer, D. E. *Anal. Chem.* **2002**, *74*, 1946.

JP811150Q